CEA-CONF-11965
FR 9500724

UNDERWATER LASER CUTTING OF METAL STRUCTURES

J.P. Alfille*, G. Pilot**, D. de Prunelé*,
C.E.A., CEN Saclay, (DPSA/ STA)*, (IPSN/SERAC)** Gif sur Yvette, France
P. Frédrick, V.S. Ramaswami, P. Muys
RADIUS ENGINEERING, Meersstraat 138B, Gent, Belgium

ABSTRACT

Stainless steel (304L) cutting tests was made in air and under 7 meters of water using CO_2 and YAG lasers. An assessment was made of how each of the lasers performed (cutting speed, quality of cut, thickness of cut attained). A study was carried out into the by-products of sectioning operations using a CO_2 laser (dross, aerosols, suspended particles in water, analysis of the gases, and chemical analysis of the aerosols). The same measurements are currently being taken in the case of the YAG laser (beam transported via optical fibre).

1. INTRODUCTION

The purpose of this study, part of a European programme, was to demonstrate and assess the feasibility of laser cutting under seven meters of water, with a view to using the process on the structures of reactor pool. Two sorts of laser were used, a CO_2 axial flux laser with a power output of 5 kW, then a pulsed YAG laser with a mean power output of 1.2 kW, with the beam transported via optical fibre. The main objectives of this study were to evaluate the cutting performance obtained in air and under water for each of the lasers (CO_2 and YAG) and to make a list of the by-products released for thicknesses of stainless steel (304L) ranging between 10 and 31 mm. Laser cutting is one of many possible methods of dismantling, it has an advantage over other methods in that it will produce less dross thanks to the very fine kerf. It is for this same reason that research is currently in hand elsewhere, mainly in Japan [1] [2].

2. GENERAL DESIGN OF THE EXPERIMENTAL DEVICE

The installation had to comply with criteria for test containment pressurization (7 meters of water) and separation of the laser source from the cutting head to simulate work in a pool. The experimental device was installed in several floors in order to comply with these conditions (Figure 1). A 500 W CO_2 laser was used for the functional tests for the entire experimental device and for the first remote cuts (thicknesses < 10mm) under a small depth of water (0.5 meter). This arrangement was replaced with the 5kW CO_2 laser in order to study greater thicknesses (> 10mm). The experimental vessel is located at ground-level, it has a volume of 0.4 m^3 (Figure 2). It consists of a underwater cutting head, a workpiece translation table with a dross box below in order to characterize the dross produced.

3. UNDERWATER CUTTING HEAD

The underwater cutting head was designed around modular mechanical optical components, and can be disassembled for maintenance (Figure 3). It consists of the following components: two lens supports with a focal length of 127 and 250 mm respectively, a rotary pneumatic valve to keep containment water out of the optical part of the head when the system is not in cutting mode, a system of interchangeable nozzles for feeding the shielding gas (O_2) needed for oxygen cutting, and a surface tracer to maintain a constant distance between the end of the nozzle and the surface of the workpiece.

4. CO_2 LASER CUTTING (CHARACTERISTICS OF THE CUT)

The tests were performed using a 5 kW CO_2 laser at a power output of 2.5 kW. Table I sets out the process parameters. Three thicknesses of stainless steel were cut in air and under 7 meters of water. Figure 4 shows the maximum cutting speeds achieved for various thicknesses of workpiece. It was observed that the cutting speed in water was approximately 40% slower than the corresponding speed in air for all thicknesses. The aspect of the cut surface was always the same (Figure 5), whether the cutting was carried out in air or in water. However, the profiles of the kerfs were more regular under water than in air. The kerf width on the top side remained almost constant at about 1 mm for cutting in both air and in water. However, the kerf width at the bottom side was about 2.5 mm in the case of cutting in air, and about 1.5 mm in water.

5. CO_2 LASER CUTTING (BY-PRODUCTS MEASUREMENTS [3])

Figure 6 gives a flow chart for the experimental device used for by-products measurements. These measurements provided a mass inventory for secondary products, including characterization of sedimented dross, aerosols and particles suspended in water, for analysing the gases released (O_2, O_3, NO, NO_X, H_2) and for supplementing these measurements by chemical analyses of deposits on sampling filters (Fe, Ni, Cr, Mn). Figure 7 gives a view of some by-products from an underwater cutting test, showing one meter of cut plate (304L), a sample of sedimented dross, the two filters Ø130 mm and Ø47 mm and the 14 filters corresponding to the inertial and diffusional spectrometer.

5.1 MASS INVENTORY FOR SECONDARY PRODUCTS RELEASED: Sedimented dross accounted for over 99% of solid mass collected in the case of cutting in air, and over 95% in the case of cutting under water. Particles in suspension account for 1.3 to 4.5% of the total mass of secondary products released. Aerosols account for 0.35 to 1% of solid mass collected in the case of cutting in air and 0.08 to 0.57% in the case of underwater cutting.

5.2 CHARACTERIZATION OF SEDIMENTED DROSS: Figure 8 gives the mass of dross produced in air and underwater per metre cut for the various thicknesses of plates. It can be seen that the mass of slag obtained in water is less than that obtained in air. For a thickness of 10 mm, there is a 10% reduction in the mass of dross underwater. However, at thicknesses of 20 and 31 mm, this reduction accounts respectively for 27% and 38%. The particle size distribution for the sediment dross reaches its maximum at 1 mm diameter.

5.3 CHARACTERIZATION OF PARTICLES SUSPENDED IN WATER: The mass of these particles per cut length increases with the plate thickness (Figure 9) and increases significantly for a thickness of 31 mm.

5.4 CHARACTERIZATION OF AEROSOLS: The mass of aerosols carried to the sampling point decreases with the depth of water. This reduction is important for the first few metres of water (Figure 10). The slope of the curve increases with the thickness of the material. The mass of aerosols increases with the cut thickness, in a almost proportionnal manner between 10 and 20 mm, and then at a faster rate for a thickness of 31 mm (Figure 11). There are two possible particle size distributions in the case of underwater cutting: particle size distribution is unimodal with a mean mass aerodynamic diameter of about 0.45 µm, or bimodal with the first modal value located between 0.07 and 0.15 µm and a second modal value in the region of 0.45 µm. In the case of underwater cutting, the mean mass aerodynamic diameter ranges between 0.4 and 0.8 µm. The mean mass aerodynamic diameter does not seem to vary with the depths of water, or with the thicknesses considered.

5.5 ANALYSIS OF THE GASES: NO is produced at a rate of 4×10^{-4} 1/min, NO_X at a rate of about 6×10^{-4} 1/min. These rates of production are quite slow

and vary only slightly with the thickness of the material and the depth of water. The rate of O_3 production ranges between 10^{-6} l/min to a few 10^{-5} l/min. The concentration of O_2 in the extraction pipe is partly caused by the O_2 needed for cutting, and partly by the O_2 from the dilution air. No production of H_2 has been detected.

5.6 CHEMICAL ANALYSIS: It can generally be seen, when one examines the ratios of Cr/Fe, Ni/Fe and Mn/Fe, that the proportion of Cr increases by a factor of 4.5 for underwater cutting and by a factor of 2 for cutting in air, the proportion of Ni increases by a factor of 4.3 and that of Mn by a factor of 2.7 for all cutting operations. The ratio of (total mass of aerosols)/(Fe+Ni+Cr+Mn) is above 1, indicating significant oxidation of the aerosols.

6. YAG LASER CUTTING (TRANSMISSION OF THE BEAM BY OPTICAL FIBRE)

The second stage of the programme has already begun. It corresponds to nuisance measurements for cutting in air and underwater using a pulsed YAG laser with a mean power output of 1.2 kW. This document presents the first results of these cutting operations. The main advantage of the YAG laser (λ=1.06 μm) is that it transmits its beam via an optical fibre, thereby avoiding the use of mirrors in the optical joints needed for transmitting a CO_2 laser (λ=10.6 μm). The corresponding test campaign will be carried out under the same conditions as for the CO_2 laser, thereby allowing a comparison of the nuisances caused by the two types of lasers.
The first cutting tests using the YAG laser were carried out in air, transmitting the beam via a 1 mm diameter optical fibre with a index jump and 25 meters in length (Figure 13). Figure 14 gives the maximum cutting speeds for the various plates thicknesses for both CO_2 and YAG lasers with a mean power output of 1 kW. Table II gives the parameters of the YAG laser. When the plate thicknesses increase from 5 to 20 mm, the maximum cutting speed decreases more rapidly in the case of the CO_2 laser than the YAG laser. The aspect of cut surfaces using the YAG laser is of high quality and without any surface irregularities, the kerf profiles are parallel (kerf width $\approx$ 1mm) over the entire length of the plates (Figure 15). Figure 16 compares the quality of the cut produced by the two lasers. The YAG laser increases the quality of the cut because of its better interaction with the material (this laser has a shorter wavelength).

CONCLUSION

This study has demonstrated the feasibility of cutting of stainless steel plate under seven meters of water using a CO_2 laser, and has provided a comparison of the relative performance achieved in air and underwater. For an incident power output of 2.5 kW, underwater, the maximum thicknesses which can be cut are 31 mm. Underwater cutting produces a finer kerf than cutting in air, and the quantity of by-products is also reduced. The second stage of the programme covers evaluation of cutting using a YAG laser with the beam transmitted via an optical fibre. Initial results have shown a clear improvement in the quality of cut obtained compared with a CO_2 laser.

REFERENCES

[1] MATSUMOTO O. *et al* "Cutting Technique for Reactor Internals by Laser Beam", Proceedings of the International Topical Meeting on Nuclear and Hazardous Waste Management, Conference SPECTRUM 90 30/09-04/10/1990, Knoxville, Tennessee, USA

[2] MIYA K. et al "Development of Laser Cutting Technique to Reactor Core Internals", Le démantèlement des installations nucléaires, politiques et techniques (SFEN),29/09-02/10/92, Avignon (FRANCE), pp 341-349

[3] J.P. ALFILLE, G. PILOT, "Découpe Sous Eau par Laser de Structures Métalliques", Rapport d'étude CEA/STA/LMS/94-DT1583/DdP/MLL, Janvier 1994

Laser power on the workpiece (W)	2500
Focal length (mm)	250
Geometry of the nozzle (mm)	1x4
Pressure and O_2 flow rate (Pa) (l/min)	4×10^5: 80
Location of focal point relative to workpiece (mm)	+13
Distance between nozzle and workpiece (mm)	1

TABLE I: Cutting parameters, 5 kW CO_2 laser

Mean laser power on the workpiece (W)	1000
Pulse length (ms)	2
frequency (Hz)	50
Focal length (mm)	100
Geometry of the nozzle (mm)	1x4
Pressure and O_2 flow rate (Pa) (l/min)	3×10^5: 80
Location of focal point relative to workpiece (mm)	0
Distance between nozzle and workpiece (mm)	1

TABLE II: Cutting parameters, 1.2 kW YAG laser

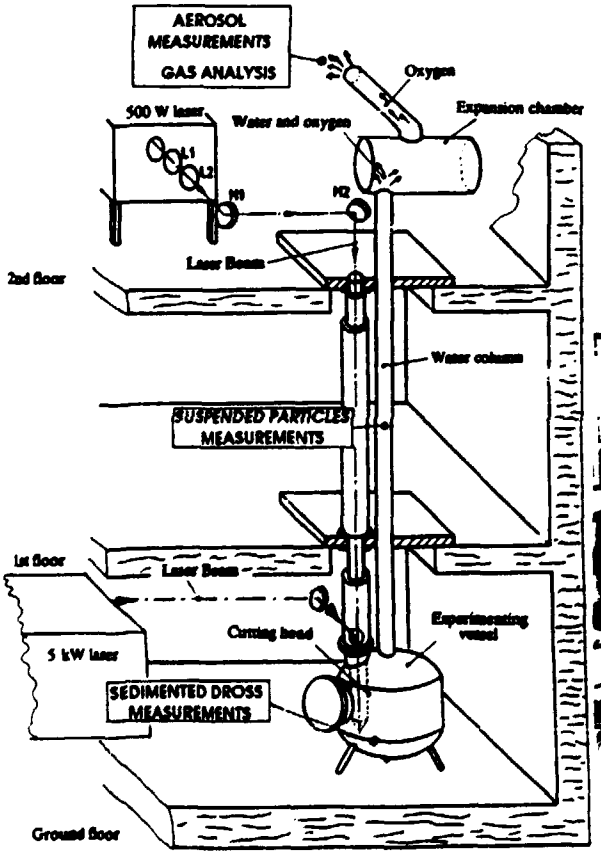

Figure 1: Diagram of the experimental device

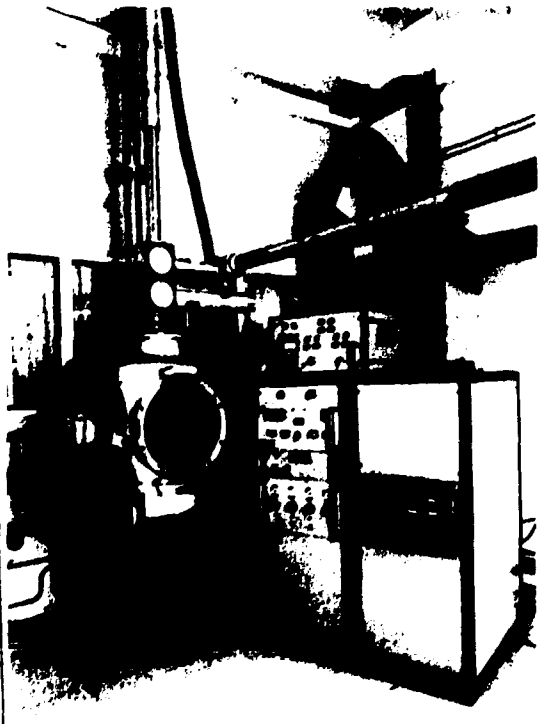

Figure 2: Experimental vessel

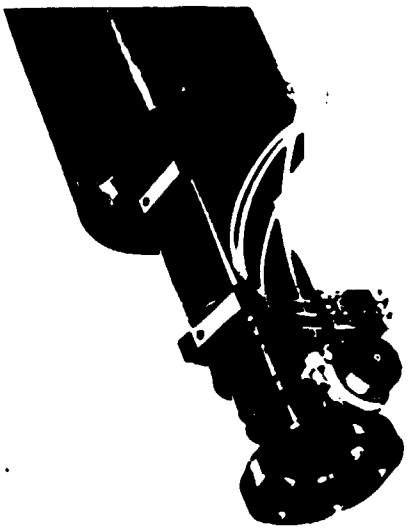

Figure 3: Underwater cutting head (CO_2 laser)

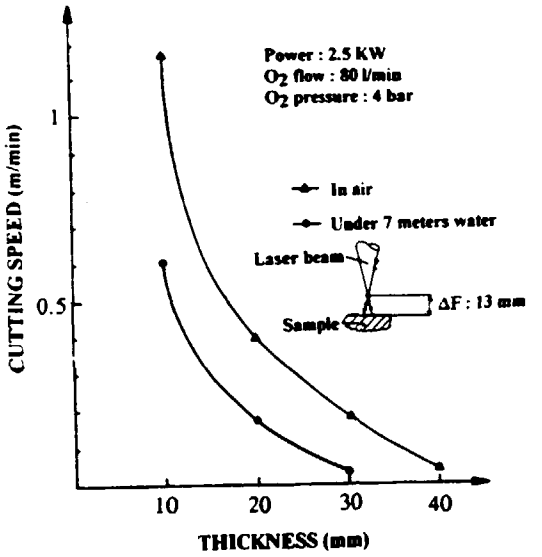

Figure 4: Maximum cutting speed versus plate thickness

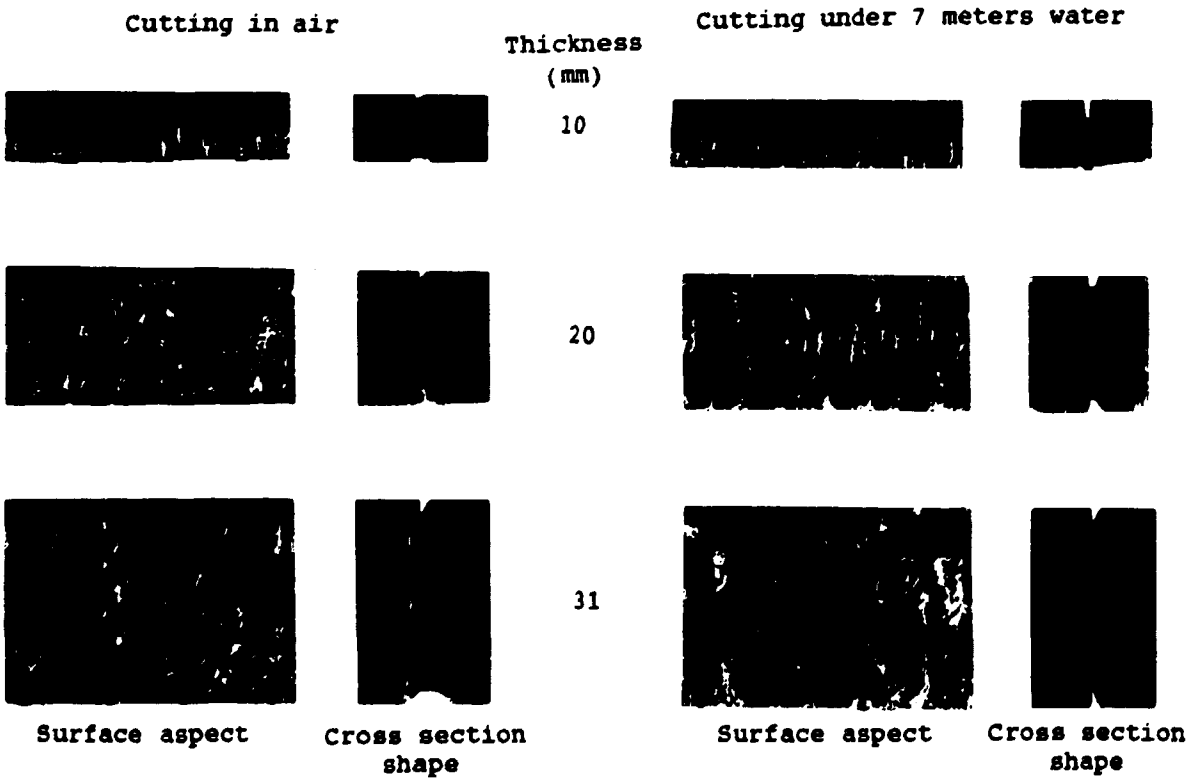

Figure 5: Appearance of cuts obtained using a CO_2 laser (304L)

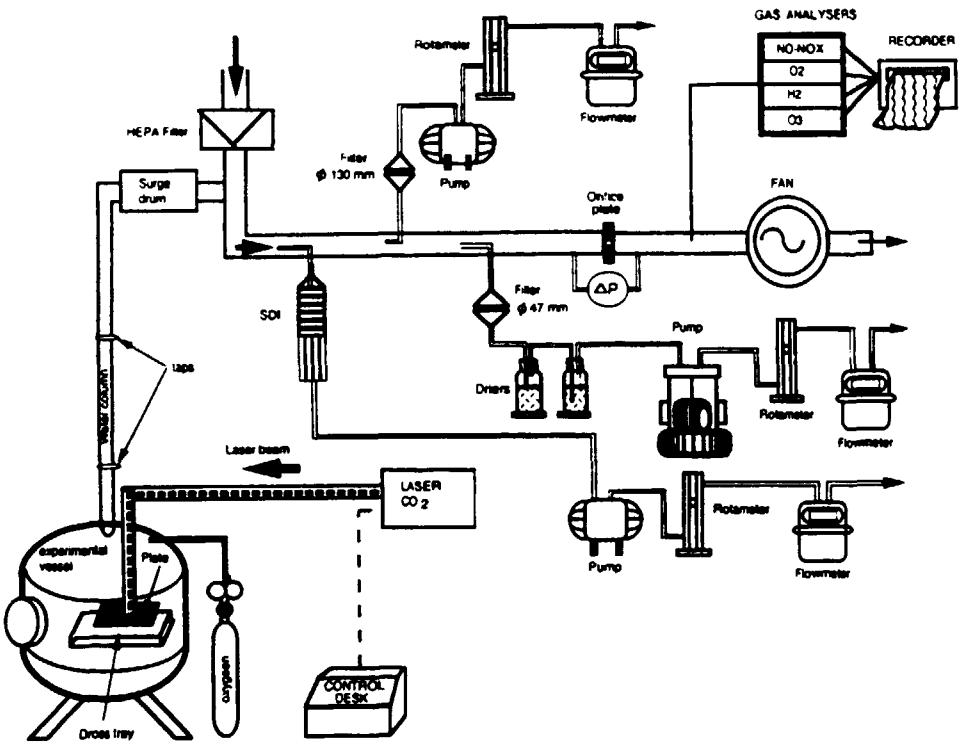

Figure 6: Diagram showing the ventilation system and associated measurements

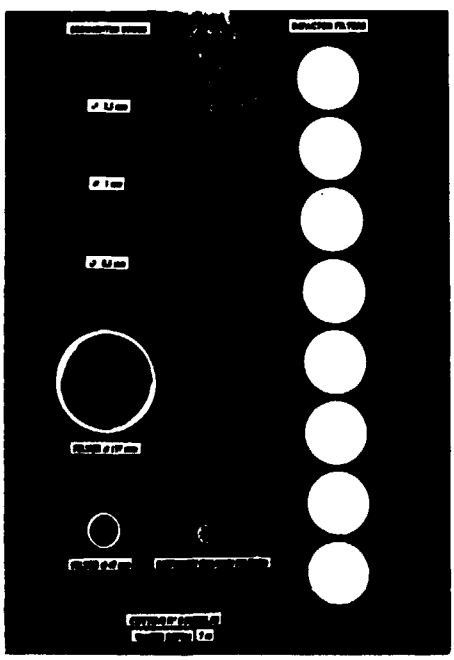

Figure 7: View of the cut plate and by-products from cutting test

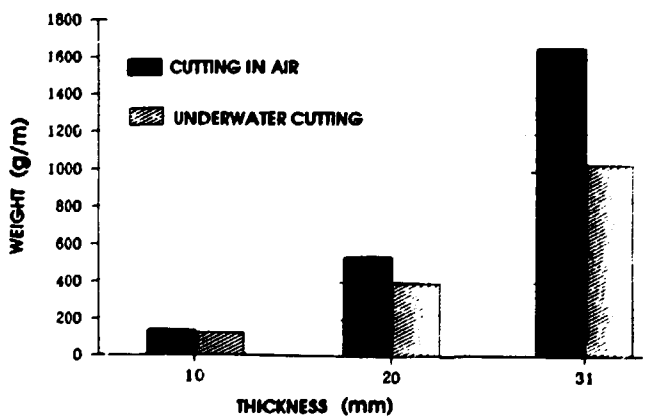

Figure 8: Dross mass versus plate thickness

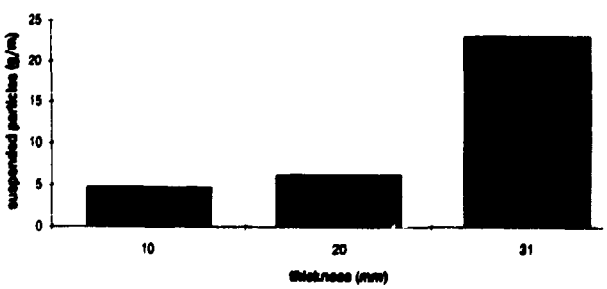

Figure 9: Production of suspended particles versus plate thickness

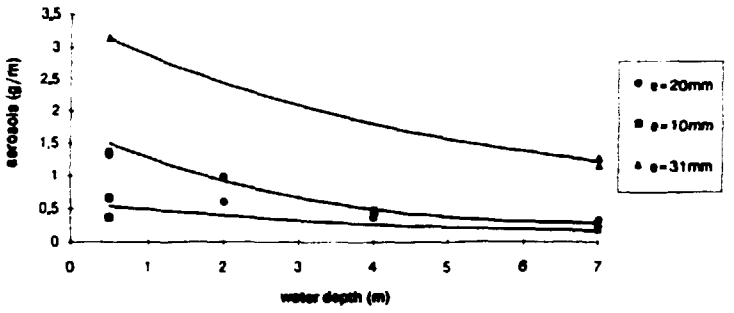

Figure 10: Production of aerosols versus water depth

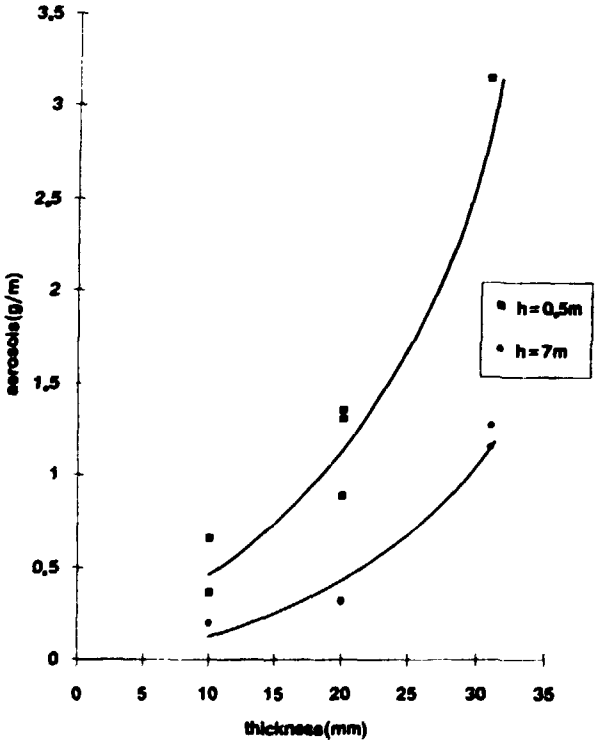

Figure 11: Production of aerosols versus plate thickness

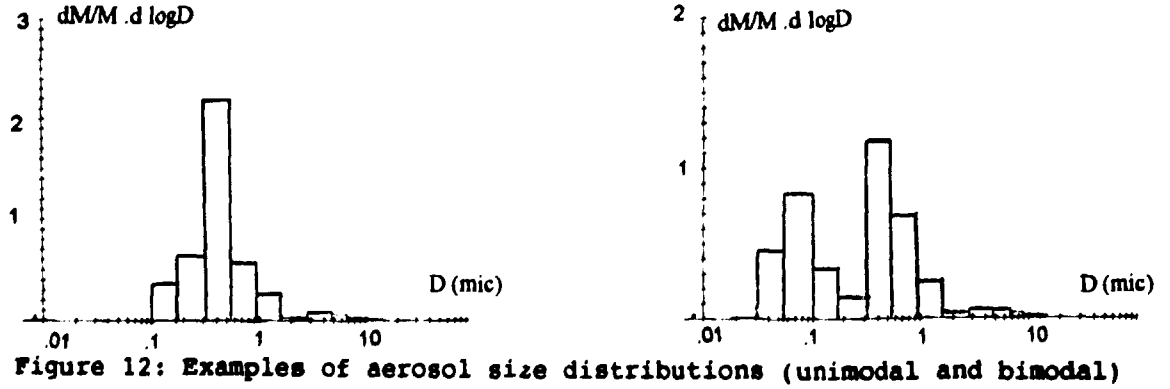

Figure 12: Examples of aerosol size distributions (unimodal and bimodal)

Figure 13: View of the YAG laser head and the system for introducing the beam into the optical fibre

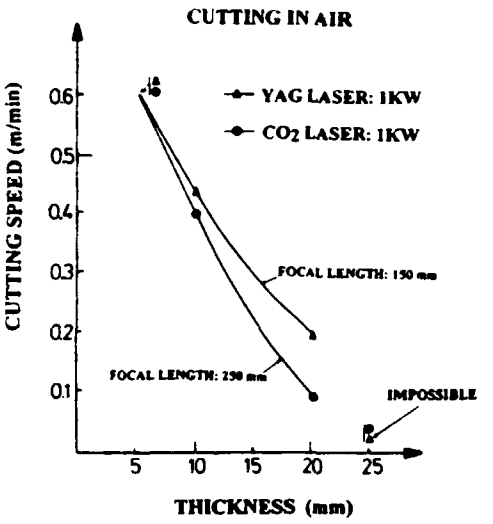

Figure 14: Maximum cutting speed for CO_2 and YAG lasers versus plate thickness

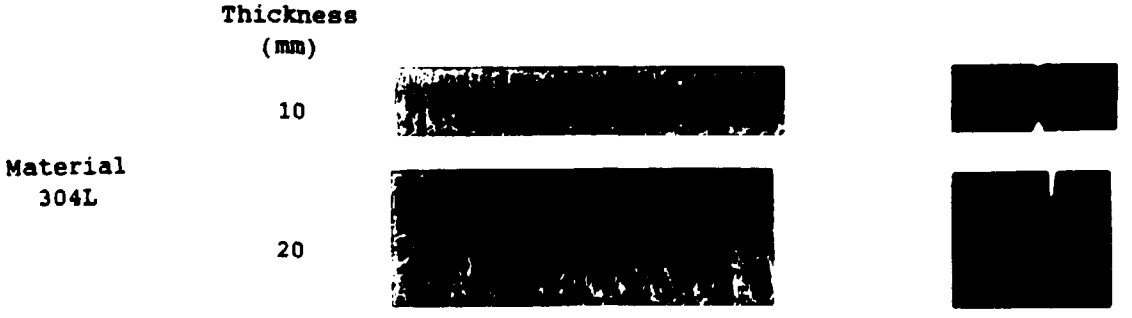

Figure 15: Appearance of cuts obtained using the YAG laser in air

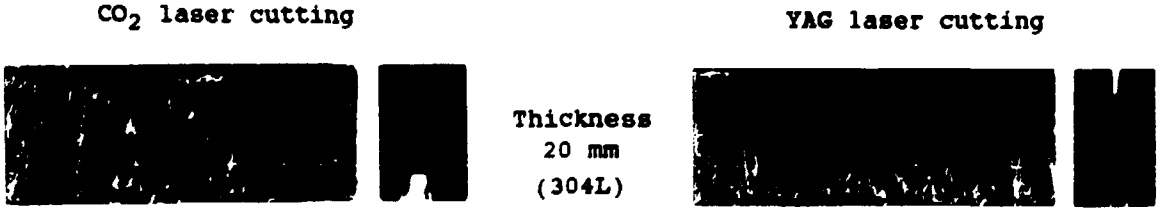

Laser power : 1KW - Cutting speed : 0.1 m/min - O_2 flow : 80 l/min

Figure 16: Comparison of the appearance of cuts obtained using the CO_2 and YAG lasers